The Nature of the Spectral Gap for Leaky Waves on a Periodic Strip-Grating Structure

Swati Majumder, David R. Jackson, *Senior Member, IEEE,* Arthur A. Oliner, *Life Fellow, IEEE,* and Marco Guglielmi

***Abstract*— The nature of the spectral gap at forward endfire for a periodic leaky-wave structure consisting of an infinite array of metallic strips on a lossless grounded dielectric layer is studied and compared with that for a simple grounded dielectric layer. The conclusions reached are expected to be valid for a general class of open periodic structures. One of the interesting features of the periodic structure is that a different branch choice is possible for each of the infinite number of space harmonics (although most of these will be nonphysical). This leads to an infinite number of steepest descent planes (SDP's) for the modal solutions, instead of only one as for the dielectric layer. As a result, one finds some interesting differences in the spectral-gap behavior, compared with that for the dielectric layer. One basic difference is that the nature of the spectral gap depends on whether or not a second space harmonic begins radiating before the main radiating harmonic is scanned to forward endfire. The spectral gap resembles that for a *lossy* dielectric layer when a second space harmonic is also radiating, and resembles that for a *lossless* dielectric layer otherwise. In addition, for the latter of these cases, the purely bound solution (which has a real propagation wavenumber and which occurs at the high-frequency end of the spectral gap) is physical only over a small frequency range, in contrast to the dielectric layer case, where that solution is present and physical at all higher frequencies. These behavioral differences are explained in detail in this paper.**

***Index Terms*— Leaky-wave antennas, leaky waves, periodic structures.**

I. Introduction

THE STUDY of spectral gaps in the propagation of leaky modes on various guiding structures has been the subject of considerable recent interest [1], [2]. The spectral-gap region is a transition region in frequency within which a guided mode changes from a physically meaningful leaky mode to a bound surface-wave mode. This transition region typically occurs as the beam radiated by the leaky mode is scanned to endfire. In the transition region, the leaky mode loses physical meaning while a surface-wave solution becomes physically meaningful. An understanding of the spectral-gap region is important in order to obtain a physical description of how the various radiating modes on a structure evolve. Although such an understanding is reasonably complete for simple structures such as a grounded slab waveguide, the spectral gap is understood relatively poorly for *periodic* structures. The goal of this paper is to obtain a basic understanding of the nature of the spectral gap for a periodic structure.

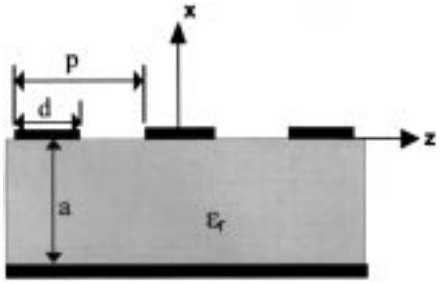

Fig. 1. Leaky-wave guiding structure consisting of an infinite array of metallic strips over a lossless grounded dielectric layer.

The specific guiding structure that will be analyzed is the periodic strip-grating structure, shown in Fig. 1. It consists of a periodic array of infinitesimally thin perfectly conducting strips on a lossless grounded substrate. Although this one-dimensional (1-D) structure is chosen for simplicity, the conclusions reached here are expected to be valid for a general class of open periodic structures, for which radiation may occur from one or more of the space harmonics.

One of the interesting features of the periodic structure is that a different branch choice for the transverse wavenumber is mathematically possible for each of the infinite number of space harmonics $k_{zn} = \beta_n - j\alpha$. That is, each wavenumber k_{xn} may be chosen to be proper (so that the space harmonic decays in the x-direction) or improper (increasing in the x-direction). This leads to an infinite number of SDP's for the modal solutions, instead of only one as for the simple dielectric layer. Although all of the solutions obtained from the different branch choices are mathematically valid, most of the solutions are completely nonphysical. For the space harmonics that are well into the slow-wave region ($|\beta_n| \gg k_0$), the solution will only have physical meaning provided that the *proper* branch choice is taken. On the other hand, for a radiating space harmonic, it is well-known that the physical choice is the *improper* one when the mode is in the forward radiating (fast-wave) region. When the frequency increases and the main radiating harmonic ($n = -1$) enters into the slow-wave region, the physical choice for this harmonic becomes the *proper* one. Hence, as frequency increases and the main radiating harmonic passes through forward endfire, physical meaning shifts between a solution where the main radiating

Manuscript received March 31, 1997; revised August 15, 1997.

S. Majumder is with the Department of Electrical and Computer Engineering, University of Houston, Houston, TX 77204-4793 USA, and with PrimeCo Personal Communication, Houston, TX 77036 USA.

D. R. Jackson is with the Department of Electrical and Computer Engineering, University of Houston, Houston, TX 77204-4793 USA.

A. A. Oliner is with Weber Research Institute, Department of Electrical Engineering, Polytechnic University, Brooklyn, NY 11201 USA.

M. Guglielmi is with the European Space and Technology Center (ESTEC), 2200 AG Noordwijk ZH, The Netherlands.

Publisher Item Identifier S 0018-9480(97)08353-1.

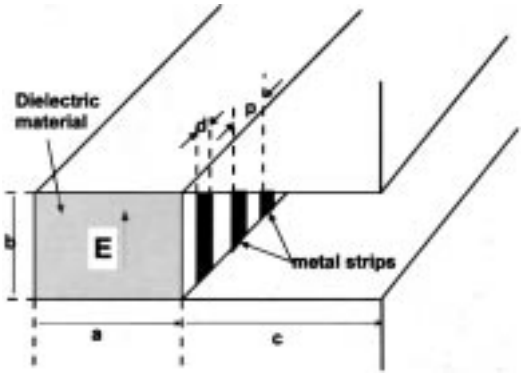

Fig. 2. Dielectric-inset waveguide leaky-wave antenna. The analysis method used for the simple structure of Fig. 1 applies for this practical antenna structure as well (see text).

harmonic is improper to one where it is proper. This transition region in frequency is the spectral-gap region.

The spectral-gap behavior of the periodic structure is complicated by the fact that there may be two space harmonics that simultaneously radiate, depending on the frequency and the strip spacing (it is assumed in the treatment here that two is the maximum number of space harmonics that can simultaneously radiate, since this would cover almost all practical cases). Because of this, there are *four* modal solutions that participate in the spectral gap, as opposed to two for the dielectric layer. One of the interesting conclusions from this study is that the nature of the spectral gap is different, depending on whether or not a second space harmonic ($n = -2$) begins radiating before the main radiating harmonic reaches forward endfire.

Although the analysis is performed for the idealized 1-D strip-grating structure, the analysis also directly applies to the dielectric inset waveguide leaky-wave antenna shown in Fig. 2. This structure is, in essence, a leaky rectangular waveguide (the polarization of the electric field in the waveguide region is labeled in the figure). If the baffle length c is infinite, the analysis is exactly the same as the one for the structure in Fig. 1; otherwise, a simple modification is necessary to account for the discontinuity at the baffle–air interface [3]. The baffle allows the higher order modes excited by the grating to decay before reaching the aperture, which results in better polarization purity of the radiated beam. This structure is a promising candidate for millimeter-wave applications due to its mechanical simplicity, low-loss behavior, and flexible radiation characteristics [4].

II. Background

In this section the basic properties of the spectral gap for a simple grounded dielectric layer are reviewed. A more complete discussion may be found in [2], [5]. This background material is included here only to provide a comparison with the spectral-gap behavior for the periodic structure.

Fig. 3 shows a steepest descent plot (SDP) of the propagation constant for the TE_2 mode of a grounded slab (the geometry is the same as in Fig. 1 without the strip grating). The steepest descent ζ plane is defined by the transformation $k_z = k_0 \sin \zeta$, where k_z is the complex propagation constant.

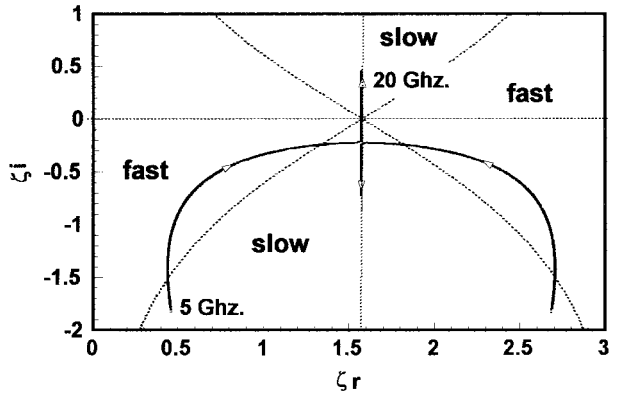

(a)

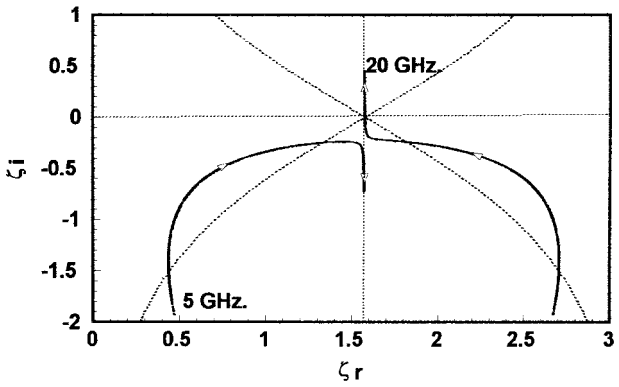

(b)

Fig. 3. Steepest descent plot showing the solution for the TE_2 mode of a grounded dielectric slab with $\varepsilon_r = 2.1$ and thickness $a = 1.29$ cm, as the frequency is scanned from 5 to 20 GHz. (a) Lossless case. (b) Lossy case with $\tan\delta = 10^{-3}$.

Fig. 3(a) shows the solution locus for a lossless layer, while Fig. 3(b) shows the locus for the same layer with a nonzero loss tangent. In both figures, the extreme SDP (ESDP) curves that cross the point $\zeta_r = \pi/2$, $\zeta_i = 0$ are shown as a pair of dashed lines. These pathes separate the slow- and fast-wave regions. Those regions adjacent to the vertical line $\zeta_r = \pi/2$ are slow-wave regions and the others are fast-wave regions. Illustrative designations are shown in Fig. 3(a).

As seen in Fig. 3(a), for a lossless dielectric layer, the leaky-mode solution crosses the ESDP as the frequency increases (see direction of arrows) and enters the spectral-gap region where the solution becomes a slow wave. Eventually it merges with the conjugate solution $k_{z2} = k_z^*$ on the $\zeta_r = \pi/2$ line. The two solutions then split to become a pair of improper surface-wave solutions. One solution travels up on the $\pi/2$ line and crosses the real axis to become a proper surface wave. The other solution continues down as a nonphysical improper surface wave. Below the splitting frequency, the conjugate solution grows exponentially in the direction of propagation, and is thus regarded as completely nonphysical.

When loss is added to the dielectric layer, these two solutions no longer meet on the $\pi/2$ line, as shown in Fig. 3(b). Instead, the original leaky-wave solution continues downward after crossing the ESDP and approaches, but never exactly

reaches, the $\pi/2$ line. The trajectory of the second solution k_{z2}, which is no longer the conjugate of the leaky-mode solution, bends upward as the solution approaches the $\pi/2$ line. This second solution crosses the real axis and shortly afterwards enters the slow-wave region, where it becomes a physically meaningful surface wave. Thus, the surface-wave solution is the continuance of the nonphysical solution.

The spectral-gap behavior of the simple grounded dielectric slab is typical of that usually seen for more complicated *nonperiodic* leaky-wave structures [2]. The purpose of this paper is to investigate the spectral-gap region of a *periodic* guiding structure, using the strip-grating structure in Fig. 1 as the model.

III. Design Considerations

The structure in Fig. 1 is designed so that the fundamental ($n = 0$) space harmonic (which resembles a perturbed TE_1 parallel-plate waveguide mode) is a nonradiating slow wave. Radiation occurs from the $n = -1$ space harmonic, which allows beam scan from backward to forward endfire.

In order to have single-beam operation over the entire scan range from backward endfire to forward endfire, the permittivity must be chosen large enough so that [3]

$$\varepsilon_r > 9 + \left(\frac{p}{a}\right)^2. \tag{1}$$

If ε_r is less than this value, the $n = -2$ space harmonic will become a fast wave (and, therefore, radiate) before the main beam can be scanned to forward endfire.

IV. Solution Procedure

A. Network Representation

The analysis used here to obtain the propagation constant of the structure is based on the transverse-resonance procedure. The key element of the structure, namely the metal-strip grating at the air–dielectric interface, is described in terms of a novel multimode equivalent-network representation [6], so that the transverse equivalent network (TEN) of the antenna is easily obtained. The TEN for the structure is shown in Fig. 4. Each transmission line connecting to the network represents the x-dependence of the fields of a particular space harmonic. The elements Z_{mn} of the coupling matrix in the TEN are given by closed-form expressions, which are derived in [7]. See [7] for detailed description.

A simple transverse-resonance equation (TRE) based on the TEN in Fig. 4 is formulated and numerically solved to obtain the complex propagation constant of the leaky wave. The details, discussed in [3], are omitted here.

B. Branch Choice for the Space Harmonics

The strip grating excites an infinite set of space harmonics with wavenumbers

$$k_{zn} = k_{z0} + \frac{2\pi n}{p}, \qquad n = \pm 1, \pm 2, \cdots \tag{2}$$

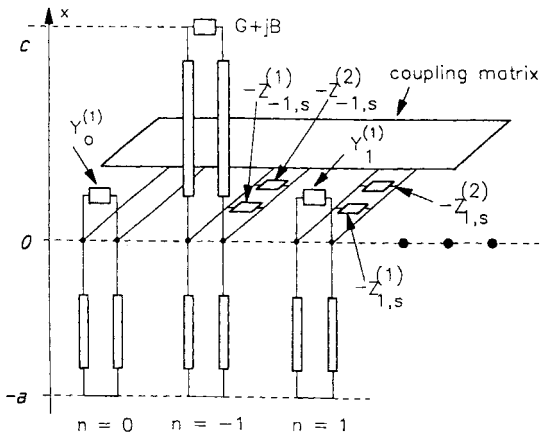

Fig. 4. TEN representation of the structure shown in Fig. 1. The grating is represented by a mutual coupling network, as described in [6].

where k_{z0} is the propagation wavenumber of the $n = 0$ space harmonic that corresponds to a perturbation of the dominant TE_1 mode of a parallel-plate waveguide structure. A different branch choice of the transverse wavenumbers

$$k_{xn} = \sqrt{k_0^2 - k_{zn}^2} \tag{3}$$

is possible for each of the infinite number of space harmonics. This contrasts with the two different branch choices for the single wavenumber k_x in the nonperiodic case. The most convenient way to study the different solutions obtained by the different choice of branches is to introduce a steepest descent variable for each of the space harmonics, so that

$$k_{zn} = k_0 \sin \zeta_n \tag{4}$$

$$k_{xn} = k_0 \cos \zeta_n. \tag{5}$$

This procedure is useful because no branch choices for the transverse wavenumber are necessary in the SDP, since both sheets of the k_{zn} plane get mapped onto the single-sheeted ζ_n plane. Both possible choices for the transverse wavenumber k_{xn} are automatically included by allowing ζ_n to assume all possible locations in the SDP.

Because there is an infinite number of space harmonics, there is an infinite number of solutions that are mathematically possible, corresponding to different branch choices for the k_{xn} wavenumbers. However, most of these solutions will not have any physical meaning. For space harmonics that have $|\beta_n| \gg k_0$, the only physical choice for the wavenumber k_{xn} is the *proper* one, for which $\mathrm{Im}(k_{xn}) < 0$. Therefore, to keep the investigation tractable, the steepest descent representation will be used for only *two* of the space harmonics: $n = -1$ and -2, since two is the maximum number of space harmonics that are likely to be in (or close to) the fast-wave region. The steepest descent representation for these two space harmonics is

$$k_{z,-1} = k_0 \sin \zeta_{-1} \tag{6}$$

$$k_{z,-2} = k_0 \sin \zeta_{-2}. \tag{7}$$

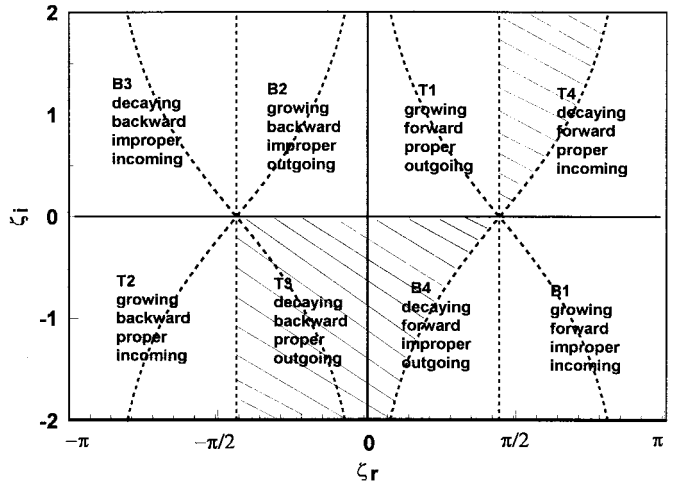

Fig. 5. The SDP, labeled to show the various characteristics in each of the different strip regions.

The -1 and -2 space harmonics are allowed to migrate freely in the corresponding SDP's, so that all possible branch choices for these space harmonics are automatically included in the investigation. All other space harmonics are chosen to be proper (decaying in the transverse x-direction).

C. Properties of the SDP

The solutions obtained from the numerical procedure will be plotted in the SDP for each of the two space harmonics that are given steepest descent representations ($n = -1$ and -2). To aid in the physical interpretation of the results, a generic SDP is first shown in Fig. 5, with labeling to indicate the nature of the region. The notation $B1$ means the mapping from the bottom (improper) sheet of quadrant one of the k_z plane; $T1$ denotes the mapping from the top (proper) sheet of quadrant one, etc. Each region is labeled to indicate whether the solution is decaying or growing in the direction of propagation, a forward or backward wave, a proper or improper wave, and an outgoing or incoming wave transversely. The regions between the ESDP curves (dashed curves) and the vertical lines at $\zeta_r = \pi/2$ and $-\pi/2$ are the regions that represent slow waves, while the regions outside the ESDP curves represent fast waves.

The four regions that correspond to growing waves are clearly nonphysical regions. Of the remaining four regions, additional criteria must be used to ascertain the physical significance of the modes. Region $T4$ has physical significance inside the slow-wave region, since this region does not correspond to radiation. Region $B4$ has physical significance in the fast-wave region, since this is an improper region that can support physical leaky modes. Region $T3$ has physical significance throughout the strip, since physical backward waves are proper, regardless of whether they are fast or slow. Region $B3$ is not physical in any region, since a physical backward wave should be proper. The shaded regions in Fig. 5 correspond to the regions where the waves are physical (all of $T3$, and parts of $B4$, and $T4$). In order for a mode to be regarded as physical, all of the space harmonics must reside in the physical regions of the SDP.

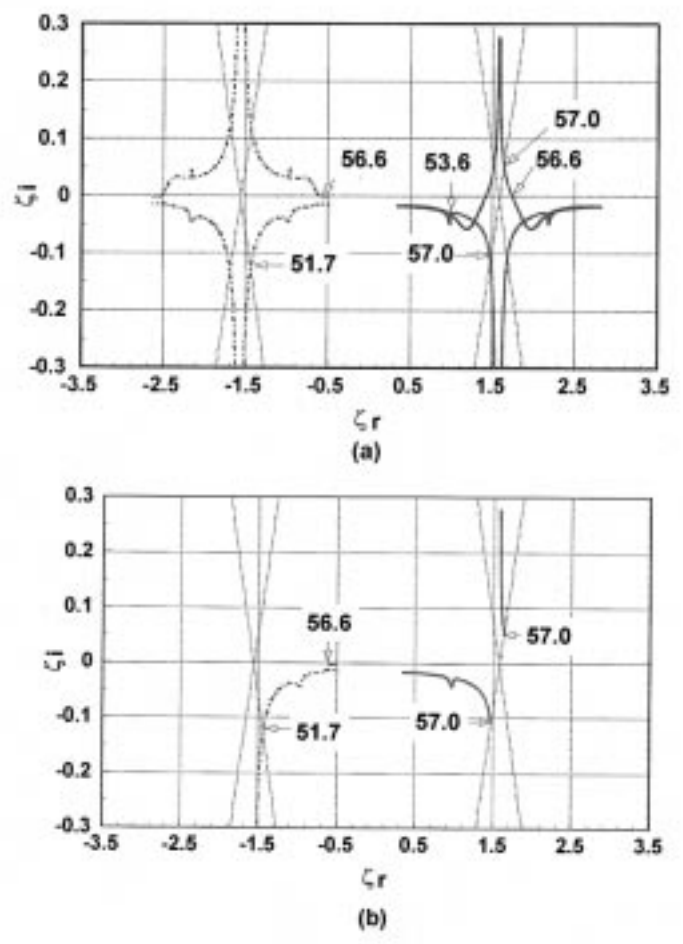

Fig. 6. (a) Steepest descent plot showing the four different solutions that are obtained from the structure in Fig. 1, as the frequency is scanned from 46 to 58 GHz. $\varepsilon_r = 9, a = 0.14$ cm, $p = 0.338$ cm, and $d/p = 0.2$. The solid curves represent the solutions for the $n = -1$ space harmonic and the dashed curves represent the solutions for the $n = -2$ space harmonic. (b) The same plot, where only the physical solutions are shown.

When part of a region corresponds to physically meaningful waves and the other part does not, the physical significance of a mode is gradually lost as the mode crosses from the physically meaningful part to the nonphysical part. This loss in physical meaning is a central feature of the spectral gap.

V. Numerical Results

Using the analysis technique mentioned in the previous section, the propagation constants for the different guided-wave solutions that were found to exist have been obtained. For all of the results shown here, the substrate thickness is $a = 0.14$ cm, the grating period is $p = 0.338$ cm, and the strip-width-to-period ratio (d/p) is 0.2. The $n = -1$ space harmonic is taken as the main radiating harmonic.

A. Two Radiating Space Harmonics

Fig. 6(a) first shows results for the case $\varepsilon_r = 9.0$ as the frequency is scanned from 46 to 58 GHz. In this case, (1) is not satisfied and the $n = -2$ space harmonic enters the fast-wave region before the $n = -1$ space harmonic is scanned

to forward endfire. Four different solutions were found from the numerical search:

1) red;
2) green;
3) magenta;
4) blue.

The solid curves show the solutions for the -1 space harmonic (ζ_{-1}) while the dashed curves show the corresponding solutions (ζ_{-2}) for the -2 space harmonic. The ESDP curves, which denote the boundaries between the fast-wave and slow-wave regions, are also shown with dashed lines (see Fig. 5).

One feature of the solutions is that they come in conjugate pairs, provided the dielectric layer in Fig. 1 is lossless. That is, if (k_{zn}, k_{xn}) is a valid solution for the set of space harmonics that compose a modal solution, then $(k_{zn}^*, -k_{xn}^*)$ is also a valid solution. A proof of this is given in the Appendix. The (red, green) and (magenta, blue) solutions form two conjugate pairs. In the SDP, the conjugate pairs are mirror images about the $\zeta_r = \pi/2$ and $\zeta_r = -\pi/2$ lines.

The red solution in Fig. 6(a) is the solution that, at lower frequencies, corresponds to the main radiating mode of the structure. This solution exhibits the characteristics of the leaky-mode solution for the *lossy* dielectric layer in Fig. 3(b), even though the dielectric in Fig. 1 is *lossless*. This is because radiation from the -2 harmonic introduces the equivalent of a loss mechanism. At higher frequencies the -1 harmonic of this solution in region $B4$ crosses the ESDP path (at 57.0 GHz) and enters the spectral-gap region. As the frequency increases, the -2 harmonic emerges from the slow-wave region near the $-\pi/2$ line in region $T3$ (crossing the ESDP at 51.7 GHz) and moves toward the origin, corresponding to a beam that scans from backward endfire toward broadside. At the frequency at which the -1 harmonic crosses the ESDP (57.0 GHz), the -2 harmonic is well within the fast-wave region (outside of the spectral gap near the $-\pi/2$ line) and, hence, there is significant radiation from this space harmonic even though the "main" radiating harmonic is entering the spectral gap.

A noticeable bump in the solution occurs at approximately 53.6 GHz, before the -1 harmonic reaches the ESDP. This bump corresponds to mode coupling between a set of space harmonics of a forward-propagating mode (power flow in the positive z-direction) and a suitably related set of space harmonics of a backward-propagating mode (power flow in the negative z-direction). In particular, the mode coupling occurs between the -2 harmonic of the forward mode and the -1 harmonic of the backward mode. It also occurs simultaneously between all space harmonics which differ by unity, such as the -1 harmonic of the forward mode and the -2 harmonic of the backward mode. The mode-coupling frequency can easily be predicted approximately from the TE_1-mode parallel-plate waveguide formula. From this simple waveguide formula, it can also be proven that the bump will occur before the -1 harmonic is scanned to forward endfire if the -2 harmonic enters the fast-wave region before the -1 harmonic reaches forward endfire.

The green solution, which is the conjugate of the red one, is a nonphysical solution since both the -1 and -2 harmonics stay within the nonphysical growing regions of the SDP, where the waves increase in the longitudinal direction of power flow.

The magenta (reddish purple) solution corresponds to the second solution in the lossy dielectric layer of Fig. 3(b). This solution starts in the nonphysical growing regions, for both the -1 and -2 harmonics, at lower frequencies. As the frequency increases, the harmonics cross the real axis at the same frequency of 56.6 GHz, and then enter the $T4$ and $T3$ regions, respectively. When the -1 harmonic first enters the $T4$ region, it corresponds to a fast surface-wave solution which is nonphysical. At a higher frequency of 57.0 GHz, the -1 harmonic enters the slow-wave region of $T4$ and the modal solution then corresponds to a physical surface-wave solution (which is complex due to leakage from the $n = -2$ space harmonic).

The blue solution, the conjugate of the magenta solution, has the -2 harmonic in a nonphysical region $B3$, since this region corresponds to an improper backward wave (physical backward waves should be proper). Hence, the blue solution is not regarded as being physically significant at any frequency.

In summary, the red and magenta solutions are the only ones for which portions of their curves lie in physically meaningful regions of the SDP, and these two solutions exchange physical meaning as the frequency increases and the modal solution changes from a leaky mode to a surface-wave mode.

Fig. 6(b) is the same plot as Fig. 6(a), except that only the physically meaningful solutions are plotted. The green and blue solutions are omitted, since they correspond to nonphysical solutions for all frequencies. For the -1 harmonic, the red solution is plotted only up to 57.0 GHz, since this solution becomes nonphysical after the -1 harmonic enters the slow-wave region in $B4$. The magenta solution is plotted only after 57.0 GHz, since this is the frequency at which the -1 harmonic enters the slow-wave region in $T4$ to become a physical surface-wave solution. For the -2 harmonic, the red solution is similarly plotted only for frequencies below 57.0 GHz. The magenta solution is plotted for frequencies above 56.6 GHz instead of 57.0 GHz, since the length of the curve is so small. The spectral-gap jump in the solutions for these two space harmonics is seen to be much larger for the -1 harmonic; for the -1 harmonic the solution changes from leaky to bound across the spectral gap, whereas the -2 harmonic remains leaky on both sides of the spectral gap.

B. A Single Radiating Space Harmonic

As the permittivity of the substrate is increased to $\varepsilon_r = 20$, the frequency characteristics of the four solutions change significantly, as shown in Fig. 7(a). In this case, (1) is satisfied and the -2 harmonic of the red solution stays within the slow-wave region of $T3$ (and very close to the $-\pi/2$ line) until the -1 harmonic reaches forward endfire at 34.15 GHz. The behavior of the $n = -1$ harmonic in the spectral gap resembles that of the *lossless* dielectric layer in Fig. 3(a). A splitting point now occurs at 34.15 GHz, where the red and green solutions merge, as do the blue and magenta solutions. After the merging of the -1 harmonic solutions, two pairs of improper surface-wave solutions emerge. The -1 harmonics

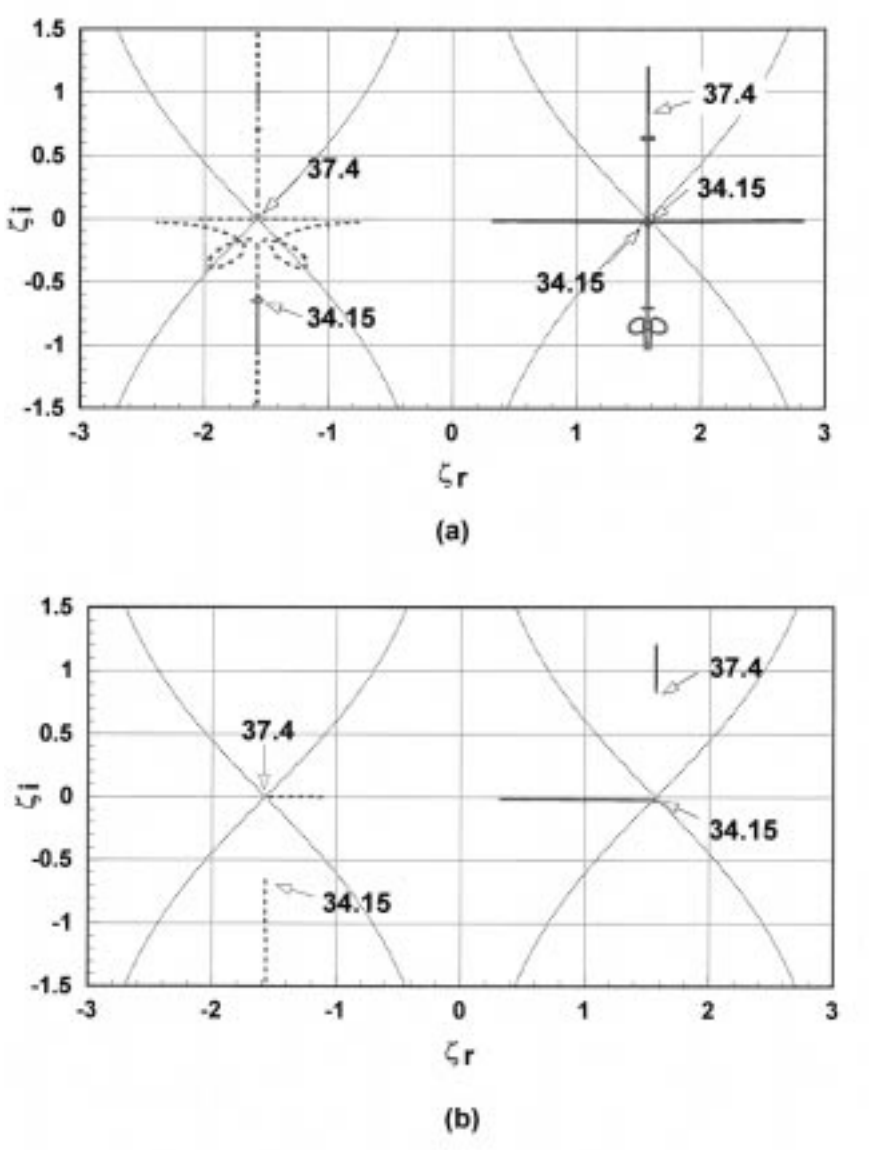

Fig. 7. (a) Steepest descent plot for the same structure as in Fig. 6, but with a higher substrate permittivity ($\varepsilon_r = 20$). The frequency scan is from 30 to 38 GHz. The behavior is seen to be different from that shown in Fig. 6. (b) The same plot, where only the physical solutions are shown.

of the red and green solutions travel down the $\pi/2$ line, and the magenta and blue solutions travel up the $\pi/2$ line and cross the real axis to become physical surface-wave solutions. The pairs of solutions are not distinguishable on the plot until the mode-coupling bump occurs, at which the solutions separate momentarily.

In Fig. 7(b) the plot is repeated with only the physical solutions being plotted. As in Fig. 6(b), the green and blue solutions are omitted, and the red and magenta solutions are plotted only in the frequency ranges for which the solutions are physical. The red solution is physical for frequencies below approximately 34.15 GHz, where the -1 harmonic enters the slow-wave region in $B4$ (almost immediately before the splitting point). The magenta solution is physical above 37.4 GHz. Below 37.4 GHz, the -2 harmonic of the magenta solution is in an improper region (above the real axis near the $\zeta_r = -\pi/2$ line) even though it is a slow (and backward) wave.

One interesting point in connection with Fig. 7(b) is that there is a noticeable frequency region of about 3 GHz (between 34.15 and 37.4 GHz) over which none of the previous four solutions have physical meaning. This initially surprising observation led to a closer investigation of the solutions near the spectral-gap region for high-permittivity substrates. It was found, after careful examination, that a *new solution* exists in the frequency range where none of the previous four solutions have physical meaning. This new solution is shown in the color cyan (light blue) in Fig. 8, which presents a magnified plot of the spectral-gap region for the $\varepsilon_r = 20$ case of Fig. 7 (the blue solution is omitted in this figure to enhance the clarity). The new solution exists between 34.15–37.4 GHz. At 34.15 GHz, the new solution merges with the green solution, and at 37.4 GHz it merges with the magenta solution. The -1 harmonic of this new solution lies on top of that of the magenta solution between 34.15–37.4 GHz. However, the -2 harmonic of the new solution is a physical wave

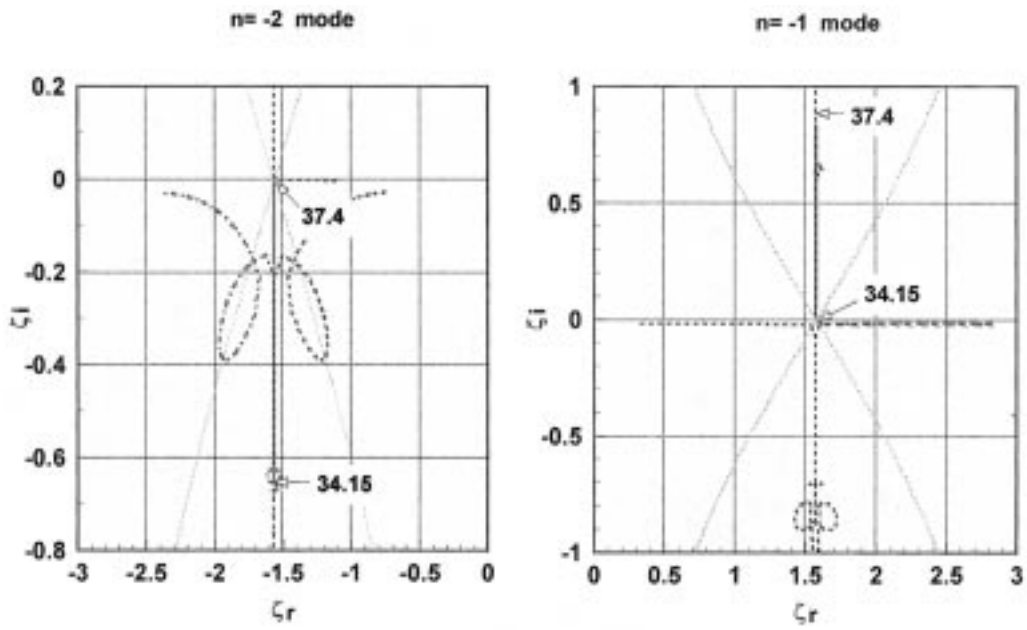

Fig. 8. A magnified plot of the spectral-gap region for the same structure as in Fig. 7 ($\varepsilon_r = 20$), showing the different solutions that interchange physical meaning as the frequency increases. The color cyan (light blue) is used to show a new solution, which does not exist for lower permittivity substrates. The blue solution is omitted for clarity.

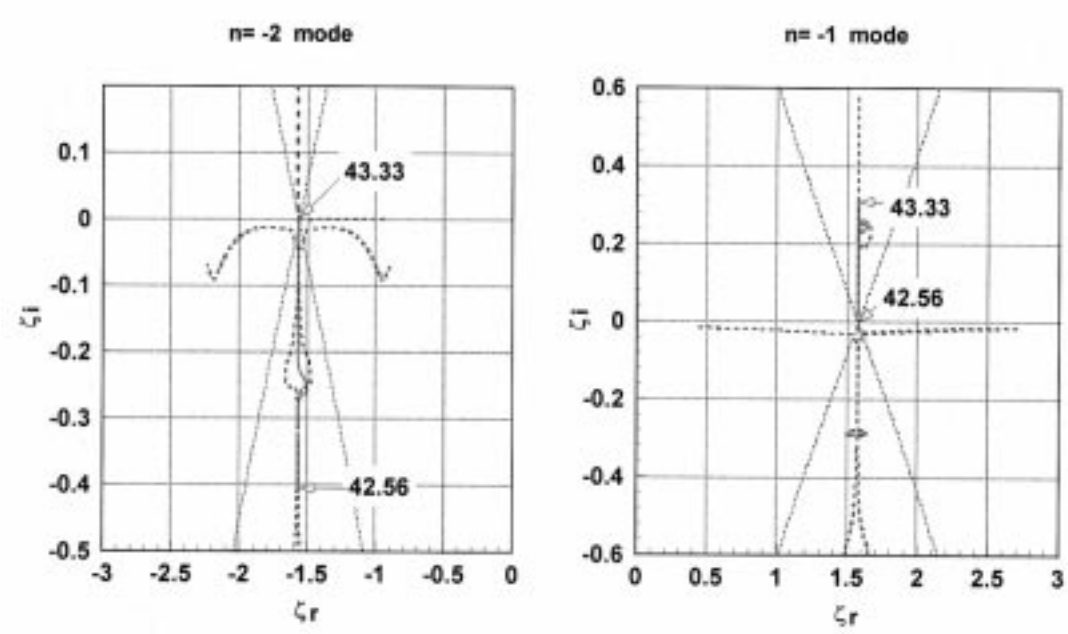

Fig. 9. A magnified plot of spectral-gap region for the same structure as in Fig. 7, but with a lower substrate permittivity ($\varepsilon_r = 14$). The frequency range over which the new solution (cyan color) exists has decreased from the case in Fig. 8.

(backward and proper) while the -2 harmonic of the magenta solution is not physical in this frequency range (it is backward and improper). Hence, only the new solution is physical in this frequency range, and the red and magenta solutions are physical outside this range, as discussed above in connection with Fig. 7(b).

C. Results for Other Dielectric Constants and Strip Widths

Fig. 9 shows the same type of result as in Fig. 8 for the case $\varepsilon_r = 14$, and demonstrates that the frequency range over which the new solution exists decreases as the permittivity is lowered. The frequency range becomes vanishingly small as the permittivity of the substrate approaches a critical value, predicted approximately by (1) when the leakage rate is small. For the lower permittivity case of Fig. 9, a noticeable mode-coupling bump is also seen in the cyan solution, where the solution momentarily departs from the $\zeta_r = -\pi/2$ and $\zeta_r = \pi/2$ lines, for the $n = -2$ and $n = -1$ harmonics, respectively. In this mode-coupling region, the cyan solution has a conjugate solution (mirror image about the $\zeta_r = \pm\pi/2$ lines) which is not shown.

Fig. 10 shows the spectral-gap behavior for two different ratios d/p of strip width to period, for the $\varepsilon_r = 20$ case. Only the region near forward endfire for the $n = -1$ harmonic is shown in this figure, corresponding to a frequency scan of 32–37 GHz. As the amount of metal in the unit cell increases, the four solutions come closer together [see Fig. 10(a)]. In particular, the red and blue solutions move closer together, as do the magenta and green solutions. In the limit, as the strip width increases so that the structure becomes a perfect parallel-plate waveguide, the four solutions merge together to become two distinct solutions.

The transition in the spectral-gap behavior as ε_r is increased from 9 to 13.5 is shown in Fig. 11, to examine how the spectral gap changes character from the type shown in Fig. 6 to the type shown in Fig. 7. The plots clearly indicate that as ε_r is increased, the mode-coupling bumps in the solution are slowly pushed out of the visible scan range. As the bumps move from the leaky regions to the $\pi/2$ line, they draw together the four solutions so that the conjugate pairs meet on the $\pi/2$ line.

D. Explanation for the New Solution Using the k_0 Versus β Diagram

For the case $\varepsilon_r = 20$, discussed in Section V-B, we found that for frequencies immediately above the spectral-gap region for the $n = -1$ space harmonic, none of the four solutions shown in Fig. 7 is physically valid. Instead, a new solution, called the cyan (light blue) solution, is the physical solution. This new solution is purely real (except in the mode-coupling region) and transversely bound, but it is present for only a small frequency range, after which the magenta solution (having a complex propagation constant) becomes physically valid. This behavior is different from that for a dielectric layer, where a purely real and bound solution is present and physically valid (as a surface wave) for all frequencies above the spectral gap. In this section, the finite range in frequency for the existence of the cyan solution for the periodic structure is explained in terms of the k_0 versus β diagram, where the need for such behavior becomes immediately evident.

The k_0 versus β diagram, which is a modification of the ω versus β diagram for closed guides (traveling-wave microwave tubes, primarily), and is also related to Brillouin diagrams, takes the form seen in Fig. 12 when applied to open structures. The quantities k_0 and β are normalized to the period p in Fig. 12, so that the abscissa is expressed simply in multiples of $\pi/2$. The diagram is periodic in $\beta p = 2\pi$, but only the first two sections are shown here. The plotted values in Fig. 12 correspond to the $\varepsilon_r = 20$ and $\varepsilon_r = 9$ cases, and the dimensional parameters, which are the same for each case, are those presented in the caption for Fig. 6. Only those solutions that are physical are included in Fig. 12.

If the solution for a particular space harmonic is located in any of the triangles (only two of which, centered at $\beta p = \pm\pi$, are shown in Fig. 12), all of the other space harmonics are also located within the triangles, since the βp values for the different space harmonics differ from each other by $2n\pi$, with n as an integer. In this case, all the space harmonics are in the slow-wave region, and the physical mode is purely bound,

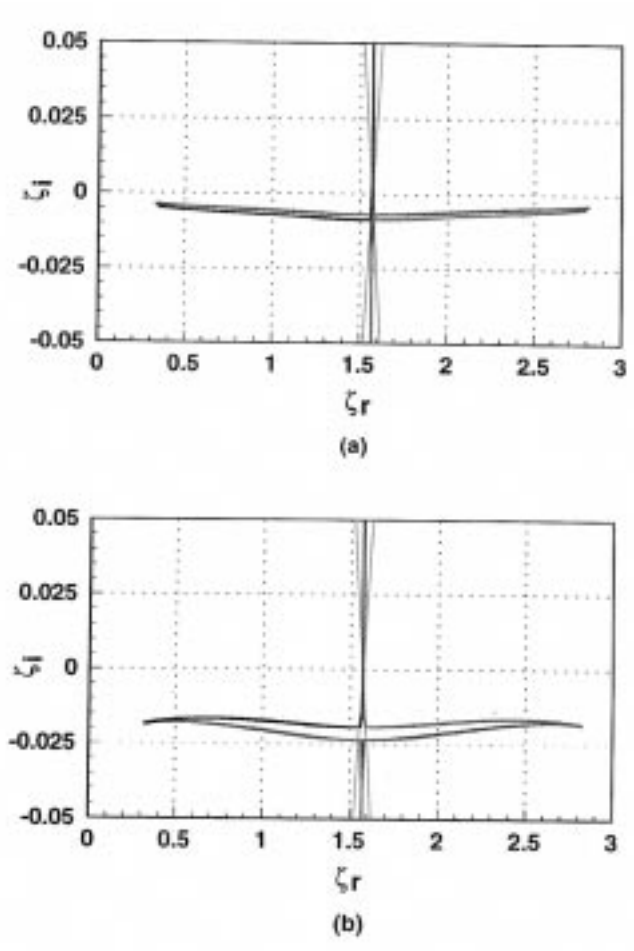

Fig. 10. Steepest descent plot showing the effect of changing the strip-width-to-period ratio d/p on the spectral-gap behavior of the structure in Fig. 1. All parameters are the same as in Fig. 7 except that the strip width d is varied to obtain different d/p ratios. (a) $d/p = 0.7$. and (b) $d/p = 0.2$. The frequency scan is from 32 to 37 GHz in both cases.

with a purely real propagation wavenumber. These triangles may, therefore, be called "bound-mode triangles." If, on the other hand, a space harmonic is located in the central region bounded by the $\pm$ 45° lines (the region that looks like a large V), the space harmonic corresponds to a fast wave. In this region, the space harmonic possesses a complex propagation constant and corresponds to a radiating leaky wave. This V-shaped region is called the "radiation region." Lastly, if a space harmonic is located in a region outside of either the bound-mode triangles or the radiation region, that harmonic is a slow wave with a complex propagation wavenumber (due to the fact that another space harmonic lies in the radiation region); its transverse field behavior is decaying, but power is coming into the structure.

For the $\varepsilon_r = 20$ case, it is seen that at lower frequencies the $n = -1$ harmonic of the red solution is in the radiation region. As the frequency is increased to 34.15 GHz, the spectral gap is reached; the red solution then loses physical significance and the cyan solution emerges as the physical surface-wave solution. Over this same frequency range the $n = -2$ harmonic lies first in the region outside of either the bound-mode triangles or the radiation region; the harmonic is slow, but

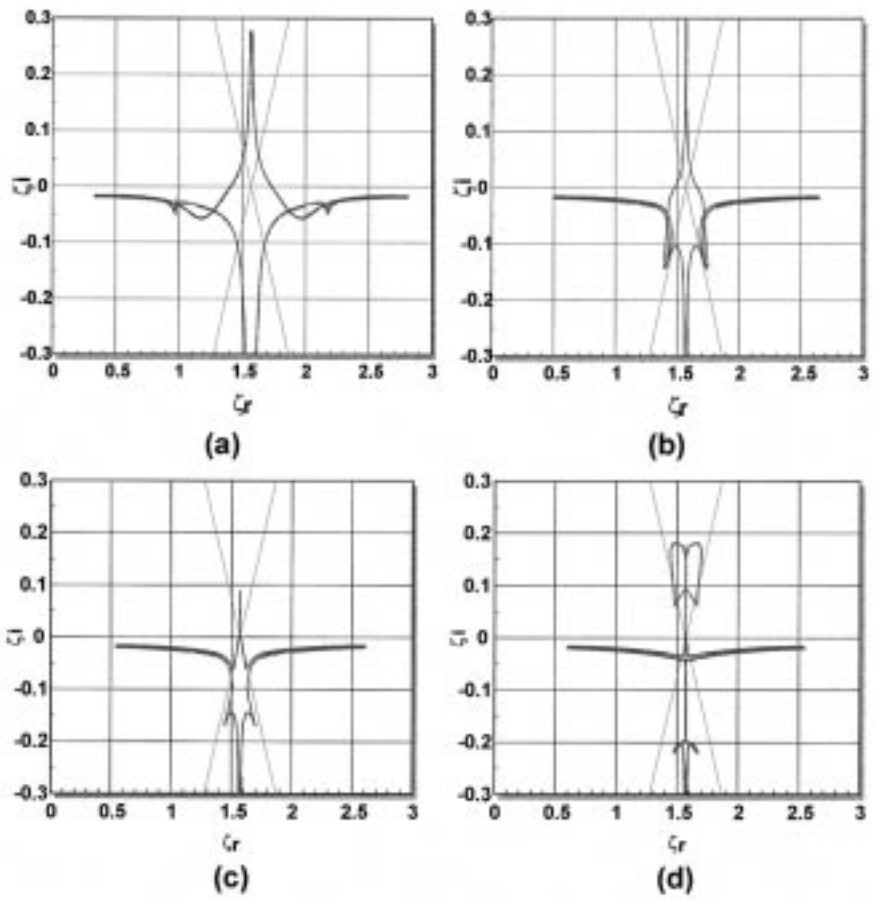

Fig. 11. Steepest descent plot showing the transformation in the spectral-gap behavior as ε_r is changed in the structure of Fig. 1. All parameters are the same as in Fig. 6 except for ε_r. (a) $\varepsilon_r = 9$. (b) $\varepsilon_r = 13$. (c) $\varepsilon_r = 13.2$. (d) $\varepsilon_r = 13.5$. The frequency scan is from 39 to 46 GHz for all parts except (a), where it is from 46 to 58 GHz.

its propagation wavenumber is complex because the $n = -1$ harmonic is radiating. At 34.15 GHz, the $n = -2$ harmonic also reaches the spectral gap, after which the solution changes from red to cyan and lies within a bound-mode triangle. Similarly, all the space harmonics will then be located within the bound-mode triangles, and the complete modal solution is thus totally bound and real (not complex) except for a small range of frequencies corresponding to mode coupling. (Mode coupling occurs at $\beta p = \pm\pi$, where a small bump, hardly noticeable, in the cyan solution is observed.) If we continue the curve for the $n = -1$ solution, it is seen that it goes out of the bound-wave triangle at 37.4 GHz, meaning that the physical solution is one that is now complex, because the $n = -2$ harmonic is now radiating. At 37.4 GHz, the $n = -2$ harmonic enters the radiation region at backward endfire. For frequencies above 37.4 GHz, the magenta solution is the physical one.

It is seen that the cyan solution represents the range of frequencies for which all the space harmonics lie within the bound-mode triangles, and that the range is finite because the $n = -2$ harmonic begins to radiate after 37.4 GHz.

The k_0 versus β plot also readily explains the behavior in Fig. 9, which holds for $\varepsilon_r = 14$. It was shown in Section V-C that for the smaller value of ε_r (14 instead of 20) the frequency range over which the cyan solution exists becomes significantly reduced (from greater than 3 GHz to less than 1 GHz). We can see from Fig. 12 that lowering the dielectric constant raises the curves (comparing the cases for $\varepsilon_r = 20$ and $\varepsilon_r = 9$), so that the curves for $\varepsilon_r = 14$ would rise higher within the bound-mode triangles, thereby reducing the cyan range within these triangles.

For the $\varepsilon_r = 9$ case, the dispersion plot in Fig. 12 is very different. As before, the -1 harmonic of the red solution is in the physical radiation region at lower frequencies. As the frequency is increased to 51.7 GHz, the -2 harmonic of the red solution also enters the physical radiation region at backward endfire. At about 53.6 GHz, i.e., at $\beta p = \pi$, a bump occurs in the red solution (hardly noticeable in this figure, but clearly visible in the SDP) due to mode coupling, as explained in Section V-A. As the frequency is further increased to 57.0 GHz the -1 harmonic reaches the spectral gap and then leaves the physical radiation region; the magenta solution then corresponds to the physical mode. The -1 harmonic of the magenta solution is complex, but not radiating, while the corresponding -2 harmonic is radiating. Above 57.0 GHz, the -1 harmonic of the magenta solution has the same character as that for the -1 harmonic in the $\varepsilon_r = 20$ case beyond 37.4 GHz.

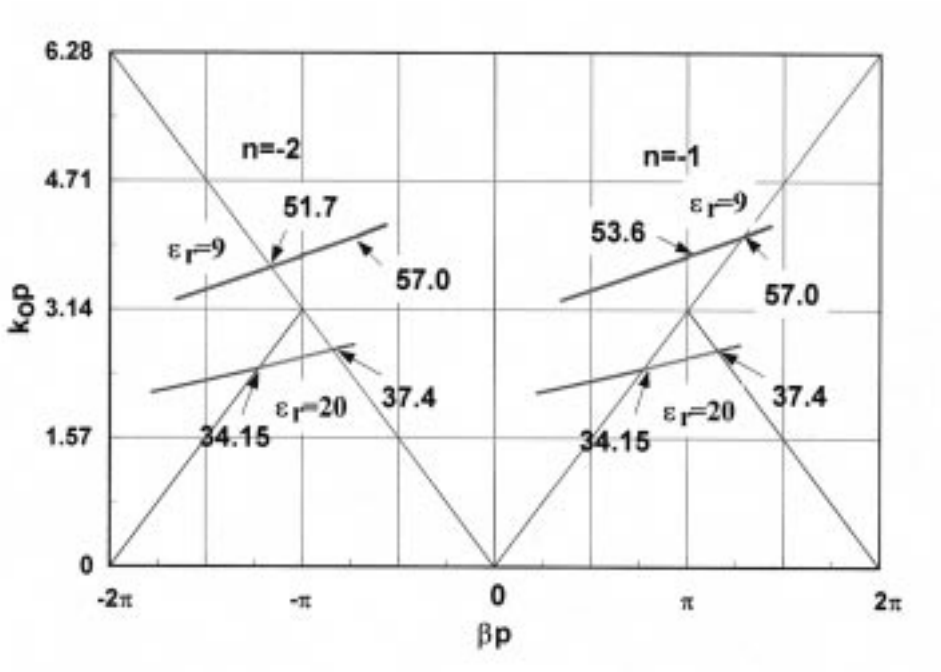

Fig. 12. $k_0 p$ versus βp diagram for the structure in Figs. 6 and 7 ($\varepsilon_r = 9$ and $\varepsilon_r = 20$). Only the physical solutions are shown in each frequency region. The $\pm 45^\circ$ lines show the physical radiation region, and the two lower triangles show the regions in which a physical solution is purely bound. For $\varepsilon_r = 20$, the plot readily shows why the cyan (light blue) solution is physically valid over only a finite frequency range.

VI. Conclusions

The spectral-gap behavior at forward endfire for a periodic strip-grating leaky-wave structure has been studied and compared with that for a simple grounded dielectric slab. The present study has revealed a number of new and interesting features. First of all, the nature of the spectral gap itself depends on whether a second space harmonic $(n = -2)$ does or does not begin to radiate before the main radiating space harmonic $(n = -1)$ reaches forward endfire. In the first case, when it does, the spectral gap resembles in form that of a *lossy* dielectric layer; in the second case, it resembles that of a *lossless* dielectric layer. Numerical calculations were made to cover both cases in detail, and also to follow the changes in behavior as one goes from one case to the other. The calculations were made using a rigorous equivalent-network representation for the strip-grating structure, which permitted rapidly convergent results to be obtained. The results were calculated and displayed on the SDP so that all possible solutions could be obtained without requiring branch-cut choices to be made beforehand.

The presence of the additional space harmonics introduced by the periodicity of the periodic structure leads to certain very important new features in the dispersion behavior. We should first recognize that there is no counterpart in the simple *lossless* dielectric layer for the case for which the $n = -2$ space harmonic is already propagating when the $n = -1$ space harmonic reaches forward endfire. The resulting spectral gap resembles in form that found for a *lossy* dielectric layer, because the additional radiating space harmonic supplies the equivalent of "loss" to the system, but the overall behavior is more complicated for the periodic structure, and of course the physics is rather different. This is the first time this case has been treated in the literature.

In the case for which the $n = -1$ space harmonic is the only radiating space harmonic when it reaches forward endfire (when the spectral gap occurs), there is also an important difference from the dielectric layer behavior. For the dielectric layer, the mode is leaky on the low-frequency side of the spectral gap, but it is purely bound (with a real wavenumber) on the high-frequency side. Furthermore, this bound solution, in the form of a surface wave, remains for all higher frequencies. In the above-mentioned periodic-structure case, similar behavior occurs in the immediate vicinity of the spectral gap, but this type of bound solution exists only for a small frequency range, until the $n = -2$ space harmonic reaches backward endfire and then radiates. Above this frequency, the $n = -1$ space harmonic remains a slow wave, but has a complex wavenumber with power coming in transversely. Again, this behavior does not have a counterpart in a simple dielectric layer.

All of these considerations, and others, were discussed and illustrated in detail in this paper.

Appendix

In this appendix the conjugate property of the modal solution for the periodic strip-grating structure is proved. That is, if the wavenumbers (k_{zn}, k_{xn}) represent a valid solution, then a second valid solution will be the set of wavenumbers $(k_{zn}^*, -k_{xn}^*)$. This establishes that a second valid solution is the mirror image of the first one about the $\pm\pi/2$ lines in the SDP.

In the SDP, the wavenumbers can be represented as

$$k_x = k_0 \cos \zeta \tag{A1}$$

$$k_z = k_0 \sin \zeta \tag{A2}$$

where

$$\varsigma = \zeta_r + j\zeta_i. \tag{A3}$$

Using (A3), (A1) and (A2) can be expanded as

$$k_x = k_0[\cos \zeta_r \cosh \zeta_i - j \sin \zeta_r \sinh \varsigma_i] \tag{A4}$$

$$k_z = k_0[\sin \zeta_r \cosh \zeta_i - j \cos \zeta_r \sinh \zeta_i]. \tag{A5}$$

In order to prove the conjugate property of the solution, it is required to show that $(k_{zn}^*, -k_{xn}^*)$ satisfies the original TRE, given by

$$\left[\frac{1}{Z_0^{(1)}}\right] - jY_0^{(2)} \cot [k_{x0}^{(2)} t] = -\frac{1}{Z_{\text{in}}^{\text{net}}} \tag{A6}$$

where the reference plane (at $x = 0$) is located immediately outside the mutual coupling network on the port corresponding to $n = 0$ (see Fig. 4). $Z_{\text{in}}^{\text{net}}$ is the input impedance looking into the mutual coupling network at that location.

For a TE mode, the characteristic impedance of the structure in the air region is given by

$$Z_0^{(1)} = \frac{\omega\mu}{k_x}. \tag{A7}$$

Hence, the transformation $k_x \rightarrow -k_x^*$ leads to the following transformation of the first term:

$$\left[\frac{1}{Z_0^{(1)}}\right] \rightarrow -\left[\frac{1}{Z_0^{(1)}}\right]^*. \tag{A8}$$

The second term gets transformed to

$$-jY_0^{(2)} \cot [k_{x0}^{(2)} t] \rightarrow -j[-Y_0^{(2)}]^* \cot [-k_{x0}^{(2)*} t] \tag{A9}$$

which is equivalent to $-j[Y_0^{(2)}]^* \cot^*[k_{x0}^{(2)} t]$ since $\tan(z^*) = \tan^*(z)$. Hence, the second term becomes

$$-jY_0^{(2)} \cot [k_{x0}^{(2)} t] \rightarrow -\{-j(Y_0^{(2)}) \cot [k_{x0}^{(2)} t]\}^*. \tag{A10}$$

All of the elements Z_{mn} of the mutual coupling network are pure imaginary for a lossless grating. These elements are constants, and are not affected by the wavenumber substitution. However, it can be assumed that

$$Z_{mn} \rightarrow -Z_{mn}^* \tag{A11}$$

since the impedance elements are purely imaginary. Hence, $Z_{\text{in}}^{\text{net}}$, the impedance looking into the $n = 0$ port of the network, gets replaced by $-(Z_{\text{in}}^{\text{net}})^*$. Therefore, in view of (A8), (A10), and (A11), if k_x is replaced by $-k_x^*$, the TRE gets transformed to

$$-\left[\frac{1}{Z_0^{(1)}}\right]^* - jY_0^{(2)*} \cot^*[k_{x0}^{(2)} t] = +\left(\frac{1}{Z_{\text{in}}^{\text{net}}}\right)^*. \tag{A12}$$

Taking the conjugate of the above equation, we obtain

$$\left[\frac{1}{Z_0^{(1)}}\right] - jY_0^{(2)} \cot [k_{x0}^{(2)} t] = -\frac{1}{Z_{\text{in}}^{\text{net}}} \tag{A13}$$

which is the original TRE. Hence, if (k_{zn}, k_{xn}) is a solution of the TRE, then $(k_{zn}^*, -k_{xn}^*)$ also satisfies the same TRE.

REFERENCES

[1] H. Shigesawa, M. Tsuji, and A. A. Oliner, "The nature of the spectral gap between bound and leaky solutions when dielectric loss is present in printed-circuit lines," *Radio Sci.*, vol. 28, no. 6, pp. 1235–1243, Nov./Dec. 1993.

[2] P. Lampariello, F. Frezza, and A. A. Oliner, "The transition region between bound-wave and leaky-wave ranges for a partially dielectric-loaded open guiding structure," *IEEE Trans. Microwave Theory Tech.*, vol. 38, pp. 1831–1836, Dec. 1990.

[3] M. Guglielmi and G. Boccalone, "A novel theory for dielectric-inset waveguide leaky-wave antennas," *IEEE Trans. Antennas Propagat.*, vol. 39, pp. 497–504, Apr. 1991.

[4] A. A. Oliner, "Scannable millimeter wave arrays," Weber Res. Inst., Polytechnic Univ. Tech. Rep. POLY-WRI-1543-88 (final report delivered to the U.S. Air Force under RADC contract F19628-84-K-0025), 1988.

[5] H. Ostner, J. Detlefsen, and D. R. Jackson, "Radiation from one-dimensional dielectric leaky-wave antennas," *IEEE Trans. Antennas Propagat.*, vol. 43, pp. 331–339, Apr. 1995.

[6] M. Guglielmi and A. A. Oliner, "Multimode network description of a planar periodic metal-strip grating at a dielectric interface—Part I: Rigorous network formulations," *IEEE Trans. Microwave Theory Tech.*, vol. 37, pp. 534–541, Mar. 1989.

[7] M. Guglielmi and H. Hochstadt, "Multimode network description of a planar periodic metal-strip grating at a dielectric interface—Part III: Rigorous solution," *IEEE Trans. Microwave Theory Tech.*, vol. 37, pp. 902–909, May 1989.

[8] M. Guglielmi and A. A. Oliner, "Multimode network description of a planar periodic metal-strip grating at a dielectric interface—Part II: Small-aperture and small-obstacle solutions," *IEEE Trans. Microwave Theory Tech.*, vol. 37, pp. 542–552, Mar. 1989.

Swati Majumder received the B.S. degree in physics from Presidency College, Calcutta, India, in 1984, the B.S. degree in electrical communication engineering from the Indian Institute of Science, Bangalore, India, in 1987, and is currently working toward the Ph.D. degree in electrical and computer engineering at the University of Houston, Houston, TX.

From 1988 to 1992, she worked at the Center for Applied Research in Electronics, Indian Institute of Technology (IIT), Delhi, India, where she was involved with surface acoustic wave (SAW) devices. In 1993, she joined Applied Electromagnetics Laboratory, University of Houston, Houston, TX, as a Research Assistant. Her main research interests are modeling and characterization of 2-D periodic leaky-wave antennas. She is also currently with PrimeCo Personal Communication, Houston, TX.

David R. Jackson (S'83–M'84–SM'95) was born in St. Louis, MO, on March 28, 1957. He received the B.S.E.E. and M.S.E.E. degrees from the University of Missouri, Columbia, in 1979 and 1981, respectively, and the Ph.D. degree in electrical engineering from the University of California at Los Angeles (UCLA), in 1985.

From 1985 to 1991, he was an Assistant Professor in the Department of Electrical and Computer Engineering, University of Houston, Houston, TX. Since 1991, he has been an Associate Professor. His research interests currently include CAD of microstrip antenna and circuits, microstrip antenna analysis and design, periodic structures, leaky-wave antennas, leakage effects in microwave integrated circuits, and bioelectromagnetics.

Dr. Jackson is a member of URSI, Commission B. He is associate editor for the IEEE TRANSACTIONS ON ANTENNAS AND PROPAGATION. He is also on the editorial board for the IEEE TRANSACTIONS ON MICROWAVE THEORY AND TECHNIQUES and *Microwave and Millimeter-Wave Computer-Aided Engineering.* He has previously served as associate editor for *Radio Science.*

Arthur A. Oliner (M'47–SM'52–F'61–LF'87) was born in Shanghai, China, on March 5, 1921. He received the B.A. degree from Brooklyn College, Brooklyn, NY, in 1941, and the Ph.D. degree from Cornell University, Ithaca, NY, in 1946, both in physics.

In 1946, he joined the Polytechnic Institute of Brooklyn (now Polytechnic University), and became Professor in 1957. From 1966 to 1974, he served as Department Head, and was the Director of its Microwave Research Institute from 1967 to 1982. He has also been a Visiting Professor at the Catholic University, Rio de Janeiro, Brazil, the Tokyo Institute of Technology, Japan, The Huazhong (Central China) Institute of Science and Technology, Wuhan, China, and the University of Rome, Italy. Since 1952, he has been a consultant to industry for IBM, Raytheon, Boeing, Hughes, AIL, Kaiser Aluminum, Rockwell, MIT Lincoln Lab., CBS Labs, etc. He was a founder of Merrimac Industries and has been on its Board of Directors since 1962. His research has covered a wide variety of topics in the microwave field, including network representations of microwave structure, precision-measurement methods, guided-wave theory with emphasis on surface waves and leaky waves, traveling-wave antennas, plasmas, periodic structure theory, and phased arrays. His interests have also included waveguides for surface acoustic waves and integrated optics and, more recently, novel leaky-wave antennas for millimeter waves and leakage effects in millimeter-wave integrated circuits. He has authored over 200 papers and has co-authored and co-edited three books.

Dr. Oliner is a Fellow of the AAAS and the Institution of Electrical Engineers (IEE) U.K., a member of the National Academy of Engineering, and a member of several commissions of the International Union of Radio Science (URSI), a past U.S. Chairman of Commissions A and D, and a member of the U.S. National Committee of URSI. He is a former chairman of a National Academy of Sciences Advisory Panel to the National Bureau of Standards (now NIST). He was President of the IEEE MTT Society, its first national lecturer, a member of the IEEE Publication Board and general chairman of three symposia. He was the recipient of the IEEE Microwave Prize in 1967, and the Institution Premium (the highest award of the IEE), in 1964. In 1982, he received the IEEE MTT-S Microwave Career Award. In 1988, a special retrospective session was held in his honor at the International Microwave Symposium. In 1990, he received the URSI van der Pol Gold Medal. In 1993, he was the first recipient of the IEEE MTT-S Distinguished Educator Award.

Marco Guglielmi was born in Rome, Italy, on December 17, 1954. He received the Laurea degree in Ingegneria Elettronica from the University of Rome "La Sapienza," Rome, Italy, in 1979, attended the Scuola di Specializzazione in Elettromagnetismo Applicato, Rome, Italy, in 1980, received the M.S. degree in electrical engineering from the University of Bridgeport, Bridgeport, CT, in 1982, and the Ph.D. degree in electrophysics from Polytechnic University, Brooklyn, NY, in 1986.

From 1984 to 1986, he was an Academic Associate at Polytechnic University, and from 1986 to 1980, he was an Assistant Professor. From 1988 to 1989, he was an Assistant Professor at the New Jersey Institute of Technology, Newark, NJ. In 1989, he joined the RF System Division, European Space Research and Technology Center, Noordwijk, The Netherlands, where he is currently involved in the development of passive microwave components for space application. His professional interests include the areas of solid-state devices and circuits, periodic structures, phased arrays, millimeter-wave and leaky-wave antennas, network representations of waveguide discontinuities and microwave filtering structures.

Dr. Guglielmi was awarded a Fulbright Scholarship and a Halsey International Scholarship Program (HISP) Scholarship.